Published OnlineFirst October 28, 2020; DOI: 10.1158/0008-5472.CAN-20-1998

Endocytosis-Mediated Replenishment of Amino Acids Favors Cancer Cell Proliferation and Survival in Chromophobe Renal Cell Carcinoma

Yi Xiao[1,2], Anja Rabien[3,4], René Buschow[1], Vyacheslav Amtislavskiy[1], Jonas Busch[3], Ergin Kilic[5,6], Sonia L. Villegas[6], Bernd Timmermann[1], Moritz Schütte[7], Thorsten Mielke[1], Marie-Laure Yaspo[1], Klaus Jung[3,4], and David Meierhofer[1]

ABSTRACT

Chromophobe renal cell carcinoma (chRCC) accounts for approximately 5% of all renal cancers and around 30% of chRCC cases have mutations in *TP53*. chRCC is poorly supported by microvessels and has markably lower glucose uptake than clear cell RCC and papillary RCC. Currently, the metabolic status and mechanisms by which this tumor adapts to nutrient-poor microenvironments remain to be investigated. In this study, we performed proteome and metabolome profiling of chRCC tumors and adjacent kidney tissues and identified major metabolic alterations in chRCC tumors, including the classical Warburg effect, the downregulation of gluconeogenesis and amino acid metabolism, and the upregulation of protein degradation and endocytosis. chRCC cells depended on extracellular macromolecules as an amino acid source by activating endocytosis to sustain cell proliferation and survival. Inhibition of the phospholipase C gamma 2 (PLCG2)/inositol 1,4,5-trisphosphate (IP3)/Ca^{2+}/protein kinase C (PKC) pathway significantly impaired the activation of endocytosis for amino acid uptakes into chRCC cells. In chRCC, whole-exome sequencing revealed that *TP53* mutations were not related to expression of PLCG2 and activation of endocytosis. Our study provides novel perspectives on metabolic rewiring in chRCC and identifies the PLCG2/IP3/Ca^{2+}/PKC axis as a potential therapeutic target in patients with chRCC.

Significance: This study reveals macropinocytosis as an important process utilized by chRCC to gain extracellular nutrients in a p53-independent manner.

Introduction

Renal cell carcinoma (RCC) accounts for approximately 4% of adult malignancies (1) and was ranked as the sixth deadliest cancer globally in 2018 (2). RCC is composed of different subtypes with distinct histologic and molecular genetic features, mainly clear cell RCC (ccRCC), papillary RCC (pRCC), and chromophobe RCC (chRCC). chRCC is derived from intercalated cells of the collecting duct and comprises approximately 5% of all renal cancers (3). It shows either a relatively transparent cytoplasm, or in about 30% of cases, eosinophilic patterns with mitochondrial accumulation (4).

Until now, only two studies have investigated the genomic and transcriptional features of chRCC (~100 cases combined; refs. 5, 6). One of the characteristic genetic features of chRCC is monosomy of chromosomes 1, 2, 6, 10, 13, 17, and often 21 (5, 7–10). The most commonly mutated genes in chRCC are *TP53* (32%), and *PTEN* (9%), and gene fusions involving the *TERT* promoter (5–7). Mutations were also observed at lower frequencies in *MTOR, NRAS, TSC1*, and *TSC2*, indicating that genomic targeting of the mTOR pathway occurred in 23% of all chRCC (5). However, both studies failed to find any clear driver mutation in over 50% of chRCC cases.

chRCC was reported to have a significantly lower microvessel density than the other two RCC subtypes, ccRCC and pRCC (11). This is further illustrated by fluorodeoxyglucose-PET (FDG-PET), which can be used to assess the glucose uptake of tumors *in vivo*; chRCC showed a significantly lower value for FDG-PET than ccRCC and pRCC (12). Hence, chRCC seems to be poorly supported by blood vessels. Because comprehensive investigations and research have focused on the more frequent ccRCC subtype, the genetic alterations and pathologic mechanism of ccRCC have been elucidated. Loss of function of the von Hippel–Lindau (*VHL*) gene was discovered as the genetic cause of ccRCC and was shown to lead to intensive metabolic aberrations (13, 14). Therefore, ccRCC has been defined as a metabolic disease (13). In contrast, even the very basic metabolic characteristics of chRCC are still unknown, and how chRCC cells adapt to nutrient-poor environments remains to be investigated.

To address these knowledge gaps, integrated proteome, transcriptome, and metabolome analyses, fluorescence imaging and whole-exome sequencing (WES) were employed to comprehensively investigate chRCC. We identified major metabolic reprogramming of gluconeogenesis, amino acid (AA) metabolism, and endocytosis. The phospholipase C gamma 2 (PLCG2)/inositol 1,4,5-trisphosphate (IP3)/Ca^{2+}/protein kinase C (PKC) pathway was proven to play a regulatory role in the activation of endocytosis and therefore to promote chRCC cell proliferation and survival. Our findings may

[1]Max Planck Institute for Molecular Genetics, Berlin, Germany. [2]Department of Biology, Chemistry, Pharmacy, Freie Universität Berlin, Berlin, Germany. [3]Department of Urology, Charité – Universitätsmedizin Berlin, corporate member of Freie Universität Berlin, Humboldt-Universität zu Berlin, and Berlin Institute of Health, Berlin, Germany. [4]Berlin Institute for Urologic Research, Berlin, Germany. [5]Institut für Pathologie am Klinikum Leverkusen, Leverkusen, Germany. [6]Institute of Pathology, Charité – Universitätsmedizin Berlin, corporate member of Freie Universität Berlin, Humboldt-Universität zu Berlin, and Berlin Institute of Health, Berlin, Germany. [7]Alacris Theranostics, Berlin, Germany.

Note: Supplementary data for this article are available at Cancer Research Online (http://cancerres.aacrjournals.org/).

Corresponding Author: David Meierhofer, Max Planck Institute for Molecular Genetics, Ihnestrasse 63-73, Berlin 14195, Germany. Phone: 4930-8413-1567; Fax: 4930-8413-1960; E-mail: meierhofer@molgen.mpg.de

Cancer Res 2020;80:5491–501

doi: 10.1158/0008-5472.CAN-20-1998

Published OnlineFirst October 28, 2020; DOI: 10.1158/0008-5472.CAN-20-1998

provide an opportunity for the development of potential therapies for chRCC.

Materials and Methods

Cell culture

The chRCC cell line UOK276 (15) was given by Marston Linehan (Center for Cancer Research at the NCI, Bethesda, MD). The ccRCC cell line 786-O and the normal kidney cell line HK2 were obtained from ATCC. The pancreatic cancer cell lines MIA PaCa-2 and BxPC-3 were provided by Ulrich Keller (Charité – Universitätsmedizin Berlin, Germany). All cell lines were cultivated at 37°C in a humidified atmosphere of 5% CO_2 in DMEM (Life Technologies) containing 4.5 g/L glucose, supplemented with 10% FBS (Silantes) and 1% penicillin–streptomycin–neomycin (PSN, Invitrogen). No *Mycoplasma* testing was performed before the experiments.

For the proliferation assays, UOK276 and HK2 cells were seeded in 96-well plates at a density of 2×10^4 cells per well in complete medium. After 12 hours, the cells were briefly rinsed and cultured in minimum essential medium (MEM) supplemented with 10% dialyzed FBS (Thermo Fisher Scientific), AAs with 0%, 1%, and 10% concentration level of MEM, and with 0 or 2.5% BSA. The number of cells was determined after 4 days.

Proteome and metabolome profiling

This study was approved by the institutional Ethics Committee (no. EA1/134/12) of Charité – Universitätsmedizin Berlin and was carried out in accordance with the Declaration of Helsinki. All participants gave written informed consent. The tumor information, proteomic and metabolomic raw data, and analysis were reported previously (10). Proteomic profiling of the UOK276 cells was performed as reported previously (16) in biological triplicates, the raw mass spectrometry (MS) data were processed and analyzed as published earlier (10).

Enzyme activity measurement

Sample preparation for a spectrophotometric assay of enzyme activity was performed as reported previously (17). In brief, approximately 5 mg samples of tumor and healthy kidney tissues were homogenized and centrifuged at 600 g at 4°C for 10 minutes. The protein concentrations of supernatants were further determined with a BCA assay (Thermo Fisher Scientific). The enzymatic activities of hexosaminidases A and B were assayed as previously described by using 4-nitrophenyl N-acetyl-β-D-glucosaminide as an artificial substrate (18). Heat inactivation of hexosaminidase A was performed by preincubation of samples for 3 hours at 48°C (19).

Stable isotopic tracer to quantify protein scavenging by endocytosis

The chRCC cell line UOK276 was initially cultured in normal DMEM (Life Technologies) supplemented with 10% dialyzed FBS and 1% PSN. Then, the medium was modified to Earle's balanced salt solution containing $^{13}C^{15}N$-labeled AAs ($^{13}C^{15}N$-AA; Cambridge Isotope Laboratories) at the same concentrations of DMEM, 10% dialyzed FBS and 1% PSN. UOK276 cells were grown for 10 doublings in $^{13}C^{15}N$-AA medium to ensure full labeling of the intercellular proteins and free AAs. After 10 doublings, the cells were seeded at a low cell density in the 6-well plate and switched to 2 mL of 1% $^{13}C^{15}N$-AA medium supplemented with 2.5% BSA. After 5 hours, the medium was collected. The cells in each well were washed once with PBS, and then 300 μL of 0.1% Triton X-100 in PBS was added. The cell lysate was collected and sonicated for 1 minute. All of the medium and cell lysate were centrifuged at 1,000 g for 10 minutes at 4°C. After centrifugation, 50 μL of supernatant was placed in a new 1.5 mL tube, and 150 μL of methanol and 10 μL of internal standard (3 μmol/L chloramphenicol) were added and vortexed for 10 minutes with a Thermomixer at 1,400 rpm, then centrifuged for 10 minutes at 18,000 g at 4°C. Finally, 20 μL of supernatant per run was injected into the LC/MS-MS for analysis.

To study the inhibitory effect of PLCG2 pathway inhibitors on endocytosis, cells were treated for 5 hours with different inhibitors [10 μmol/L 5-(n-ethyl-N-isopropyl)-amiloride (EIPA), 30 μmol/L U73122, 100 μmol/L 2-aminoethoxydiphenyl borate (2-APB), 30 μmol/L BAPTA-AM and 3 μmol/L bisindolylmaleimide I (BI)], and then the total AAs in the cells and medium were extracted following the above-described protocol and injected into the LC/MS-MS for relative quantification.

Endocytic BSA uptake assay

The endocytic uptake assay was performed similarly to a previously reported protocol (20). Briefly, BxPC-3, MIA PaCa-2, 786-O, UOK276, and HK2 cells were seeded in a 96-well Screenstar Plate (Greiner) and grown for 24 hours. After starvation for the following 15 hours in serum-free DMEM with 1% PSN, a self-quenched BODIPY dye conjugate of BSA (DQ-Red BSA, 0.1 mg/mL, Molecular Probes) was added to each well. After incubation for 30 minutes, the cells were rinsed with PBS and fixed with 4 % formaldehyde for 10 minutes. Cells were then washed in PBS and stained with 1 μg/mL Hoechst 33242 for 15 minutes and washed again before proceeding to imaging acquisition. All experimental steps were performed using multichannel pipettes and stock solutions to ensure minimal well-to-well variations. Fluorescence imaging was performed using the Zeiss Celldiscoverer 7 operated by ZEN blue3.1. Cells were imaged using a 20×/0.95 Plan-Apochromat-objective with a 1× postmagnification and a Axiocam 506 camera with 2 × 2 binning, resulting in a lateral pixel size of 0.453 μm/pixel. The definite focus 2 hardware autofocus was used to ensure constant object–objective distances. A total of 88 positions (∼50 % well surface) in three channels (for Hoechst 33432, DQ-Red BSA, and transmitted light) were captured automatically. Cells were identified on the basis of nuclear Hoechst signal using a fixed fluorescence threshold. The software module dilated the identified nuclear regions of interest by 20 pixels (=0.906 μm) and quantified the red fluorescence intensities, area, and geometrics associated within that target region.

To validate the role of the PLCG2 pathway in endocytosis, UOK276 cells were seeded in a 96-well plate and grown for 24 hours. After starvation for 15 hours with serum-free DMEM with 1% AA and 1% PSN, DQ-Red BSA (0.1 mg/mL) was added to the wells and incubated for 30 minutes. Fluorescence imaging and analysis was performed as described above.

WES

DNA was isolated from the remaining pellets after metabolite extraction, with a DNA purification kit according to the manufacturer's protocol (QIAmp DNA Mini Kit for Tissues, QIAGEN). In brief, the pellets were lysed with proteinase K, and the RNA was removed by RNase. The RNA-free genomic DNA was then purified and eluted on QIAamp Mini spin columns for library preparation. The library preparation was performed according to Agilent's SureSelect protocol (SureSelectXT Human All Exon V5, protocol version B4 August 2015) for Illumina paired-end sequencing, as reported previously (16).

Published OnlineFirst October 28, 2020; DOI: 10.1158/0008-5472.CAN-20-1998

DNA reads were aligned to the human reference genome hg19 using BWA (bwa-mem 0.7.17-r1188) and sorted, and duplicates were removed using Picard (v2.17.11). Somatic single-nucleotide variants were detected using established pipelines based on VarScan2 (21) and functional annotation of the variants based on Ensembl v.70 was performed using annovar (22). Somatic indels were detected using SAMtools and Dindel (23).

Analysis of The Cancer Genome Atlas RNA-seq data

The Cancer Genome Atlas [TCGA; ID: KICH (chromophobe); KIRC (clear cell)] RNA sequencing (RNA-seq) data were obtained from UCSC Xena (https://xenabrowser.net/; ref. 24). Accurate transcript quantification of chRCC ($n = 66$) and ccRCC ($n = 533$) was based on the RNA-seq by expectation maximization method (25).

Statistical rationale and pathway analyses

For proteome and metabolome datasets, a two-sample *t* test was performed. Multiple test correction was performed by Benjamini—Hochberg (BH) with an FDR of 0.05 by using Perseus (v1.6.0.2; ref. 26). For comprehensive proteome data analyses, gene set enrichment analysis (GSEA, v3.0; ref. 27) was applied to determine whether an *a priori* defined set of proteins shows statistically significant, concordant differences between chRCC and kidney tissues. Only proteins with valid values in at least 6 of 9 samples in at least one group, with replacement of missing values from the normal distribution for the other group, were used (10). GSEA default settings were applied, except that the minimum size exclusion was set to 10 and Kyoto Encyclopedia of Genes and Genomes (KEGG) v6.2 was used as a gene set database. The cut-off for significantly regulated pathways was set to a $P \leq 0.01$ and an FDR ≤ 0.05.

Data availability

The datasets generated in this study are available as Supplementary Files, and the raw data files were reported previously (10) and are available in the following repositories.

WES files can be accessed via https://www.ncbi.nlm.nih.gov/sra with the accession number PRJNA413158. Proteomics raw data have been deposited in the ProteomeXchange Consortium via the Pride partner repository (28) with the dataset identifier PXD019123. Metabolomics data have been deposited in the publicly available PeptideAtlas repository with the identifier PASS01250 and can be downloaded via http://www.peptideatlas.org/PASS/PASS01250.

Results

Proteome and metabolome profiling of chRCC

To comprehensively understand the metabolic features of chRCC, we employed two systematic omics approaches, MS-based proteome and metabolome profiling, in nine chRCC and adjacent healthy kidney tissue samples (**Fig. 1A** and **B**). chRCC derives from the distal tubules, distal and proximal nephrons are known to be metabolically distinct, but we want to emphasize that they colocalize in any given section of the kidney, which serve as healthy controls in our study.

A total of 26,839 peptides and 3,575 proteins were identified in chRCC samples and adjacent healthy kidney tissues from 9 patients, both at a FDR of 1%. 56.9% (2,034) of these proteins were quantified in at least six out of nine samples. Between different samples, the Pearson correlation ranged from 0.659 to 0.921 in chRCC and 0.770 to 0.955 in kidney tissues (Supplementary Fig. S1A). Principal component analysis revealed that the first component distinguished the chRCC specimens and kidney tissues, but with two outliers, the chRCC tumor of patient 4 (C4) and the kidney tissue from patient 9 (K9; Supplementary Fig. S1B). These results indicate high variability within tumor samples, most likely due to differences in microenvironmental conditions or the tumor heterogeneity. A *t* test with the BH correction for multiple testing was performed to identify significantly (FDR ≤ 0.05) altered proteins between chRCC and the controls. Altogether, 983 significantly regulated proteins were identified, with 390 proteins upregulated and 593 downregulated in chRCC (**Fig. 1C**). Among these significantly changed proteins, fructose-1,6-bisphosphatase (FBP1), which was shown to oppose ccRCC progression (29), decreased more than 16-fold in the tumors. PLCG2 was increased by over 59-fold in chRCC, and its high transcript level has been considered as a potential biomarker for chRCC (6). Thus, our proteomic analysis could verify known molecular signatures of RCC and serve as a source dataset for subsequent computational analyses.

GSEA revealed several significantly ($P \leq 0.01$ and FDR ≤ 0.05) regulated KEGG pathways in chRCC versus healthy tissues (**Fig. 1D**). The pathways upregulated in chRCC compared with normal tissue included the proteasome, ubiquitin-mediated proteolysis, lysosome, and phagocytosis. In contrast, pathways involved in energy supply chains and nutrient homeostasis, such as lipid metabolism, glutathione metabolism, peroxisome, glycolysis and gluconeogenesis, and AA metabolism, were significantly downregulated in chRCC (**Fig. 1D**).

Metabolome profiling targeting a panel of 366 metabolites was performed. Metabolite identification was based on three strict criteria to exclude false-positive results: (i) the correct retention time, (ii) up to three multiple reaction monitoring (MRM) transitions, and (iii) a matching MRM ion peak ratio of tuned pure metabolites as a reference (17). With this strategy, 144 metabolites were identified and quantified (**Fig. 1E**). Statistical analysis using a two-sample *t* test with the BH (FDR of 0.05) correction for multiple testing revealed 9 significantly ($P < 0.01$) increased and 19 significantly decreased metabolites in chRCC relative to kidney tissues (**Fig. 1E**). The top three significantly upregulated metabolites are all related to glutathione metabolism (including both oxidized and reduced glutathione and the glutathione precursor gamma-glutamyl cysteine; **Fig. 1E**), consistent with a previous study performed in chRCC (30). Interestingly, a similar pattern was reported in other RCC subtypes, including ccRCC (14), pRCC (31), and renal oncocytoma (16, 32). Thus, the increase of glutathione has been proposed as a hallmark of kidney cancer and targeting glutathione metabolism can be exploited as a specific treatment strategy (33).

Gluconeogenesis is completely stalled in chRCC

The KEGG pathway "glycolysis and gluconeogenesis" was significantly reduced in chRCC (**Fig. 1D**). This pathway describes two opposing metabolic functions: the generation of pyruvate from glucose and vice versa. Thus, the details of this metabolic pathway was examined, and the results showed that all glycolytic enzymes were either unchanged or slightly increased, indicating increased glycolysis in chRCC (**Fig. 2A**). All enzymes involved solely in gluconeogenesis were dramatically decreased in chRCC, including pyruvate carboxylase (PC, 124-fold), phosphoenolpyruvate carboxykinase 1 (PCK1, 96-fold), PCK2 (996-fold), aldolase B (ALDOB, 922-fold), and FBP1 (29-fold; **Fig. 2A**). The two aldolase isoforms, A (ALDOA) and C (ALDOC), which were increased in chRCC, have a high affinity for fructose-1,6-bisphosphate (F-1,6-BP) to promote glycolysis, whereas the greatly diminished isoform B has a low affinity for F-1,6-BP and hence promotes the conversion from glyceraldehyde-3-phosphate to F-1,6-BP (34). Furthermore, the decrease in PC, which is the main entry point for pyruvate into the tricarboxylic acid cycle, shows that the

Published OnlineFirst October 28, 2020; DOI: 10.1158/0008-5472.CAN-20-1998

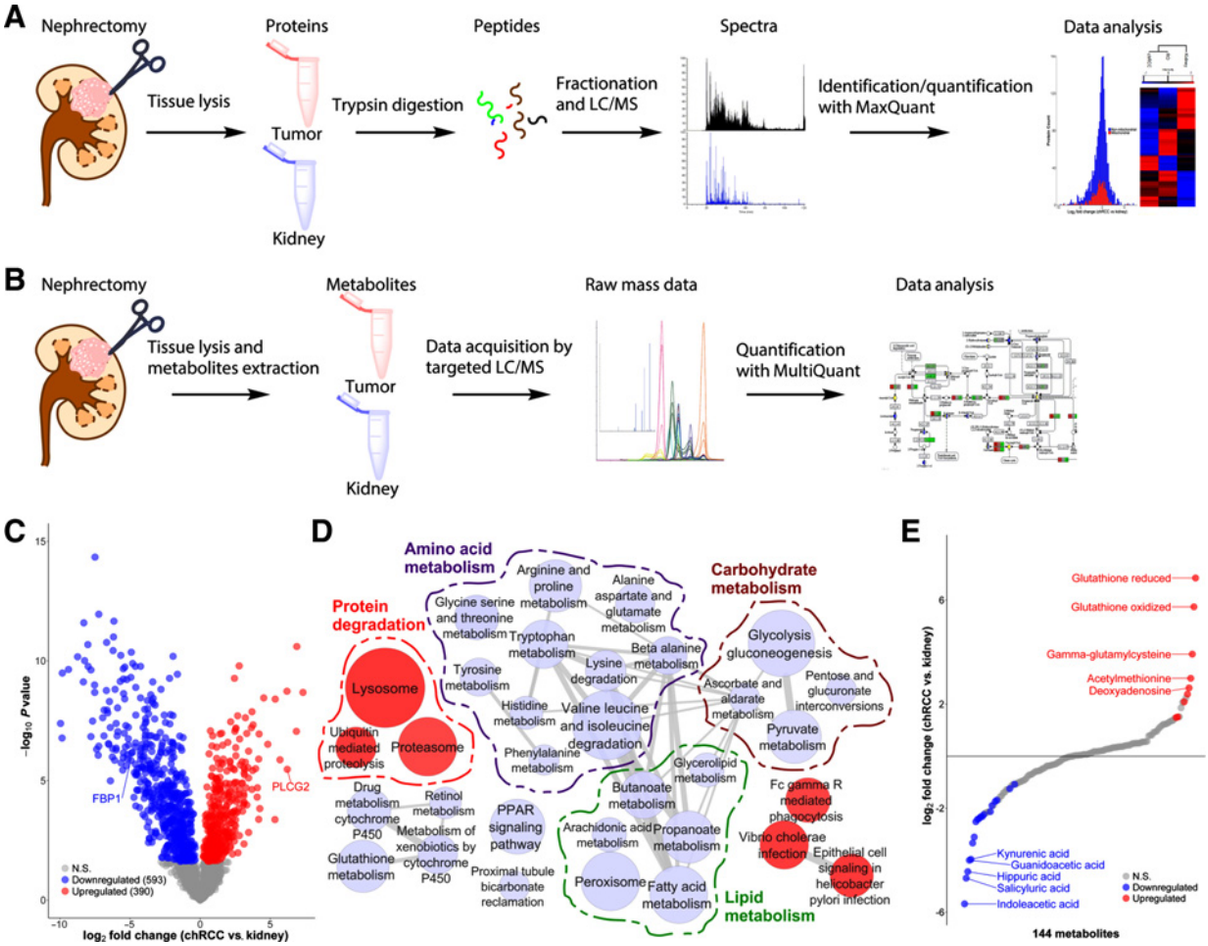

Figure 1.

Proteome and metabolome profiling of chRCC. **A,** The proteome workflow involves tissue lysis of the tumor and kidney samples, followed by protein digestion with trypsin, peptide fractionation, LC/MS-MS analysis, and label-free quantification. **B,** The metabolome workflow involves tissue lysis of the tumor and kidney samples and metabolite extraction, followed by data acquisition with a targeted LC/MS-MS approach and relative quantification of the peak areas. **C,** A volcano plot of $\log_2$ abundance ratios of chRCC versus kidney tissues ($n = 9$) against the $-\log_{10}$ (P value) of the proteome. Altogether, 390 proteins were significantly upregulated and are shown in red; 593 proteins were significantly downregulated and are shown in blue. **D,** Protein pathway analysis of chRCC versus kidney controls. Indicated are significantly ($P \le 0.01$ and FDR ≤ 0.15) enriched (red) and decreased (blue) KEGG pathways in chRCC. Gray lines connect overlapping pathways. Similar pathways are circled by a dotted line, such as decreased AA, lipid, and carbohydrate metabolism and increased protein degradation. **E,** The distribution of the fold changes of 144 metabolites in our cohort ($n = 9$) of chRCC versus kidney tissues. Significantly (FDR < 0.01) upregulated and downregulated metabolites are shown in red and blue, respectively. N.S., not significant.

tumors rely on lactate fermentation, which was also indicated by significantly increased lactate dehydrogenase A (LDHA; 3-fold) protein levels in chRCC. An analysis with chRCC transcriptome data extracted from TCGA (5) showed similar regulatory effects, with a significant depletion of all transcripts involved in gluconeogenesis (**Fig. 2B**). Stalled gluconeogenesis can be considered as one of the most relevant metabolic changes observed in this tumor and a hallmark of chRCC.

Previously, we discovered that chRCC has a diminished oxidative phosphorylation capacity (10), combined with a higher abundance of glycolytic proteins, a typical phenomenon of the classical Warburg effect. Hypoxia-inducible factor (HIF), a master transcriptional regulator, can regulate the Warburg effect, glycolysis, and gluconeogenesis in various tumor types and normal tissues (35, 36). In ccRCC, because of *VHL* loss of function, HIF accumulates and enhances the transcription of its target genes. These target genes are associated with crucial oncogenic pathways, including glucose uptake, glycolysis (e.g., glucose transporter, *GLUT*), cell proliferation (e.g., *EGFR; TGF*), and angiogenesis (e.g., *VEGF*; refs. 37–40). Despite the lack of known genetic alterations of HIF, we wondered whether HIF is involved in the regulation of glycolysis and gluconeogenesis in the context of chRCC. Analyzing and comparing the transcriptome data of ccRCC and chRCC (both datasets from TCGA) showed that all HIF signature targets in ccRCC had increased expression relative to that in the normal kidney (**Fig. 2C**). In contrast, these genes were almost all downregulated in chRCC, except for VEGFA, which displayed lower expression in chRCC than in ccRCC (**Fig 2C**). These results indicate that HIF is not involved in the glucose metabolism of chRCC.

Taken together, the above results show that chRCC has disrupted glucose metabolism, in which glycolysis is slightly upregulated while

Published OnlineFirst October 28, 2020; DOI: 10.1158/0008-5472.CAN-20-1998

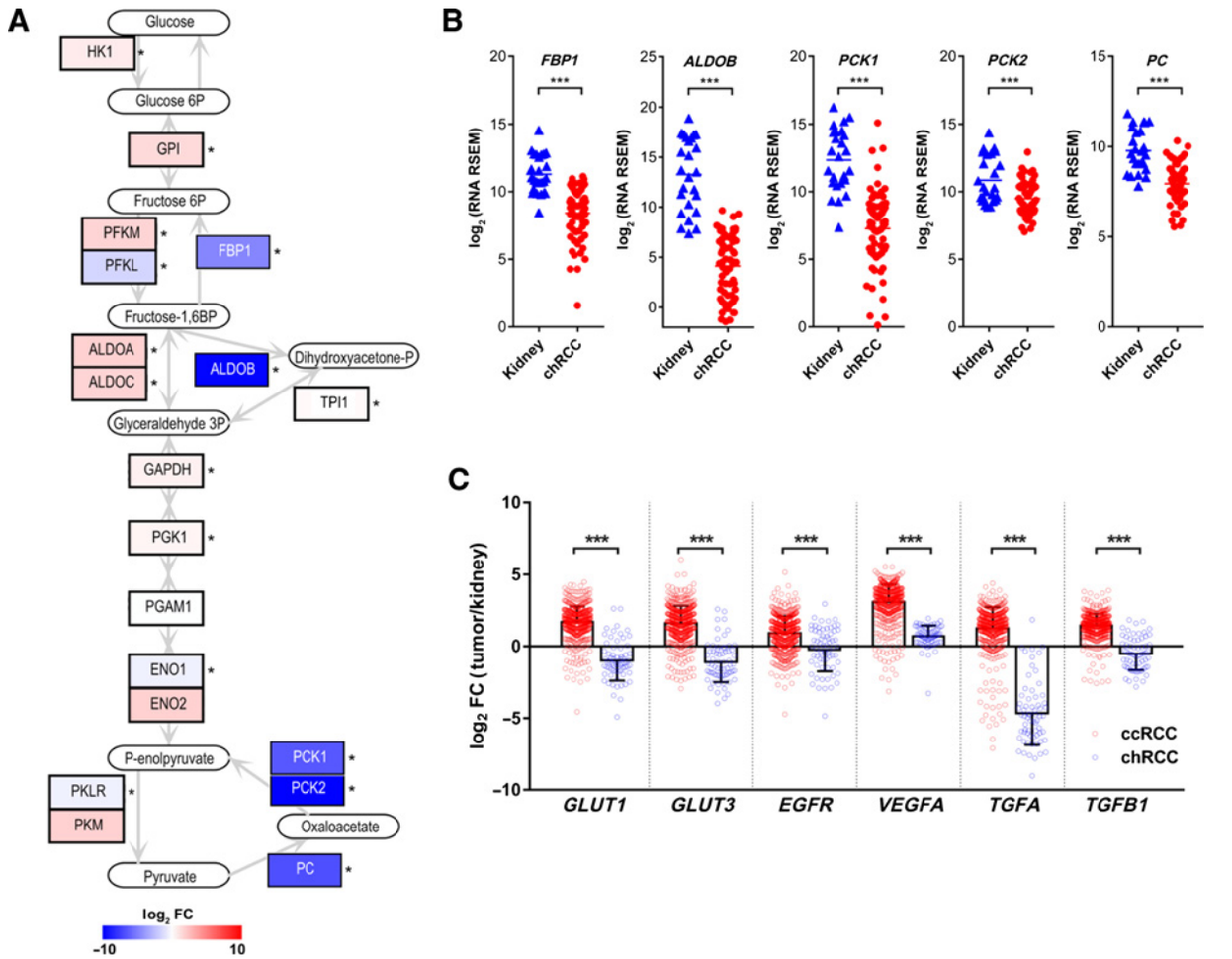

Figure 2.

Gluconeogenetic alterations in chRCC. **A,** Protein abundances of the metabolic pathways glycolysis and gluconeogenesis in chRCC. Log_2-fold changes are displayed between chRCC and kidney tissues. Upregulated proteins, red; downregulated proteins, blue. *, significantly regulated proteins. **B,** Transcripts (from TCGA) of gluconeogenic genes between chRCC tumors ($n = 66$) and controls ($n = 25$). *FBP1*, fructose-1,6-bisphosphatase 1; *ALDOB*, fructose-bisphosphate aldolase B; *PCK1*, phosphoenolpyruvate carboxykinase, cytosolic; *PCK2*, phosphoenolpyruvate carboxykinase, mitochondrial; *PC*, pyruvate carboxylase. The data were calculated by RNA-seq by expectation maximization method. **C,** Transcript fold changes (log_2) of the main HIF targets in chRCC ($n = 66$) and ccRCC ($n = 533$) versus healthy controls. **B** and **C,** ***, $P < 0.001$ by a two-tailed Student *t* test.

gluconeogenesis is entirely stalled. Unlike in ccRCC, HIF is not involved in the regulation of these alterations in chRCC.

chRCC features depletion of metabolic intermediates and pathways involved in AA metabolism

At the proteome level, 10 distinct pathways involved in AA metabolism were found to be significantly downregulated in chRCC (**Fig. 1D**). In total, 95 of 114 proteins involved in AA metabolism showed decreased abundance (average 22-fold; **Fig. 3A**). Altogether, 19 proteins decreased by over 40-fold (BBOX1, HPD, PSAT1, ACY1, DDC, ALDH3A2, CHDH, MAOB, FTCD, EHHADH, DPYS, DMGDH, ALDH4A1, SHMT1, ABAT, ASS1, AGMAT, BHMT, and GATM; **Fig. 3A**), indicating a major metabolic change. In addition, six pathways associated with fatty acid metabolism were significantly downregulated (**Fig. 1D**), including fatty acid metabolism and the peroxisome, the main organelle for fatty acid oxidation. Metabolites involved in AA metabolism were among the most depleted in chRCC, matching the decreased protein abundances of AA pathways (**Fig. 3B–G**). These included guanidoacetic acid (metabolism of multiple AAs, glycine, serine, threonine, arginine, and proline, 16-fold), kynurenic acid (tryptophan metabolism, 16-fold), indoleacetic acid (tryptophan intermediate, 51-fold), ureidopropionic acid (β-alanine metabolism, 6-fold), hippuric acid (glycine metabolism, 22-fold), salicyluric acid (glycine metabolism, 26-fold) and acetylglutamine (glutamine metabolism, 5-fold; **Fig. 3B–G**). Interestingly, all AAs were either unchanged or negligibly increased; the only exception was glycine, which was nonsignificantly decreased in chRCC (Supplementary Fig. S2). Selected AAs and intermediates were mapped together with the corresponding enzyme abundances onto their pathways to indicate upstream or downstream derivation (Supplementary Fig. S3A–S3C). These results indicate that all metabolic processes that generate AAs were significantly diminished in chRCC, but surprisingly, the amounts of the standard AAs remained unchanged.

Published OnlineFirst October 28, 2020; DOI: 10.1158/0008-5472.CAN-20-1998

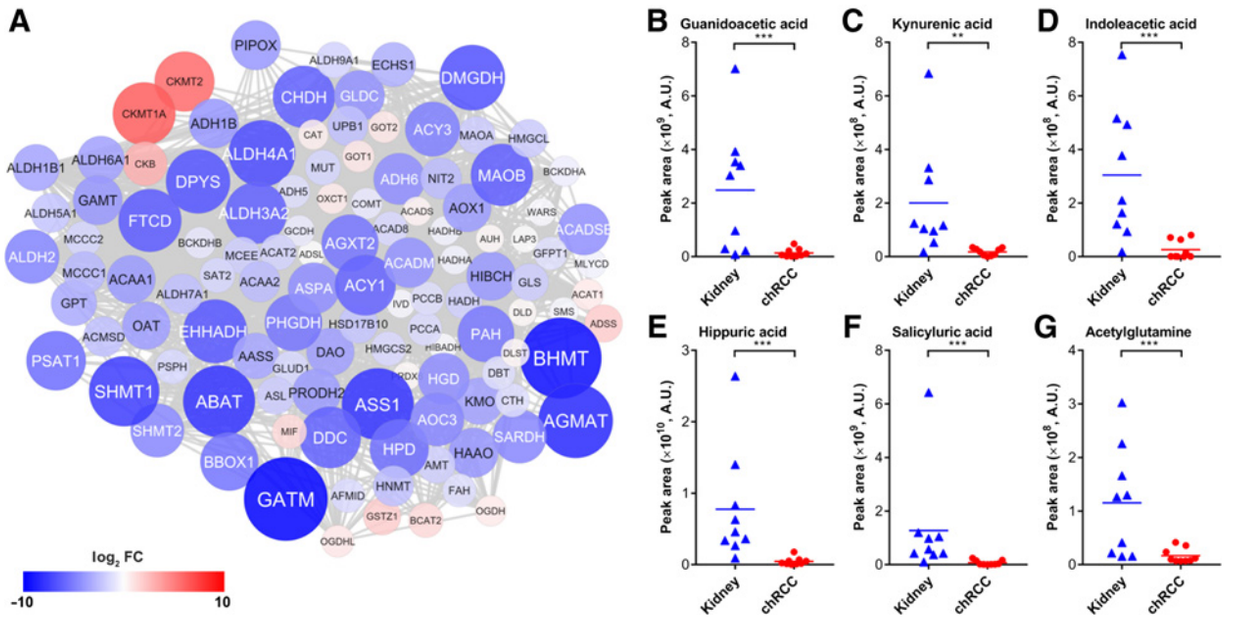

Figure 3.

Regulation of AA metabolism in chRCC. **A,** A protein–protein interaction network was created to elucidate the regulation of the entire AA metabolism pathway in chRCC. The colors of the nodes correspond to the protein expression fold change comparing chRCC and healthy kidney tissues. Red, higher expression in chRCC; blue, lower expression in chRCC. The size of the nodes corresponds to the absolute protein expression fold change. **B–G,** The relative abundances of six selected AA intermediates are shown for kidney tissues and chRCC. **B,** Guanidoacetic acid. **C,** Kynurenic acid. **D,** Indoleacetic acid. **E,** Hippuric acid. **F,** Salicyluric acid. **G,** Acetylglutamine. **B–G,** **, $P < 0.01$; ***, $P < 0.001$ by a two-tailed Student t test. A.U., arbitrary units.

chRCC cells feed on extracellular macromolecules via endocytosis to sustain proliferation and survival

chRCC is poorly supported by blood vessels in terms of nutrient supply and has been shown to have a significantly lower glucose uptake than other RCC types (11, 12). In addition, our analyses showed that AA metabolism was significantly downregulated in chRCC (**Figs. 1D** and **3**), but all AA levels remained unchanged (Supplementary Fig. S2). We hypothesized that chRCC cells could preferentially internalize and catabolize external macromolecules as a source of AAs. Indeed, one pathway related to endocytosis (Fc gamma R-mediated phagocytosis) and three protein degradation pathways (lysosome, ubiquitin-mediated proteolysis, and proteasome) were significantly upregulated in chRCC (**Fig. 1D**). V-type proton ATPases and Rab GTPases play essential roles in endosome formation, maturation, transport, and fusion with lysosomes (41, 42). Most of these proteins were significantly upregulated in chRCC relative to kidney tissues (**Fig. 4A**). Interestingly, a few exceptional proteins, including three V-type proton ATPases (ATP6V1B2, ATP6V0A1, ATP6V1C1) and two Rab GTPases (RAB29, RAB5C), were more highly expressed in kidney tissues than in chRCC tumors (**Fig. 4A**), which might suggest different roles of these proteins in the endocytic process. Two lysosome markers, lysosomal-associated membrane protein 1 and 2 (LAMP1 and LAMP2), were upregulated by 3- and 7-fold, respectively (**Fig. 4A**). These metabolic changes indicate that extracellular biomass recruitment and protein degradation are preferentially used to obtain mass and nutrients in chRCC.

To further investigate whether the increased abundances of lysosomal proteins correlate with increased enzymatic activities in chRCC, we measured the activity of two lysosomal enzymes, hexosaminidase A and B. These enzymes are involved in the breakdown of gangliosides and were both found to be significantly increased in chRCC (**Fig. 4B** and **C**).

Next, we asked whether macromolecule supplementation enhances the growth rate of chRCC cells and whether this can be mirrored by alterations in the abundances of proteins in endocytosis related pathways. Therefore, we evaluated the proliferation of the chRCC-derived cells UOK276 (15) and normal kidney cells (HK2) under different AA and BSA concentrations. Overall, both UOK276 and HK2 cells grew significantly faster under all AA concentrations when supplemented with 2.5% BSA, and only the UOK276 cells grew equally well when supplied with 10% of the AA level present in minimum essential medium (**Fig. 4D** and **E**). UOK276 cells proliferated normally even at a low AA concentration of 1% and the addition of 2.5% BSA, whereas HK2 cells significantly reduced their growth rate under the same condition. This result suggests that UOK276 cells have higher potential to utilize BSA to compensate for AA depletion. Proteome profiling of UOK276 cells supplemented with 1% AAs and the addition of 2.5% BSA versus complete medium revealed a significant increase in endocytosis (transferrin endocytosis and recycling, Reactome) and lysosome (KEGG) pathways (**Fig. 4F**; Supplementary Table S1). Enzymatic activity measurement and comparison of the lysosomal hexosaminidases A and B of UOK276 cells between the previously mentioned conditions further confirmed that external macromolecules triggered internalization and degradation pathways to break down macromolecules enzymatically via endocytosis (**Fig. 4G** and **H**), which indicates the adaptation of chRCC cells to nutrient-poor conditions. To comprehensively validate the increased endocytosis rate in chRCC cells, a quantitative fluorescent image–based assay was applied. This assay exploits a self-quenched BODIPY dye conjugates of BSA (DQ-Red BSA), which only dequenches and starts to show a red fluorescent signal after being digested. Live-cell fluorescence imaging

Published OnlineFirst October 28, 2020; DOI: 10.1158/0008-5472.CAN-20-1998

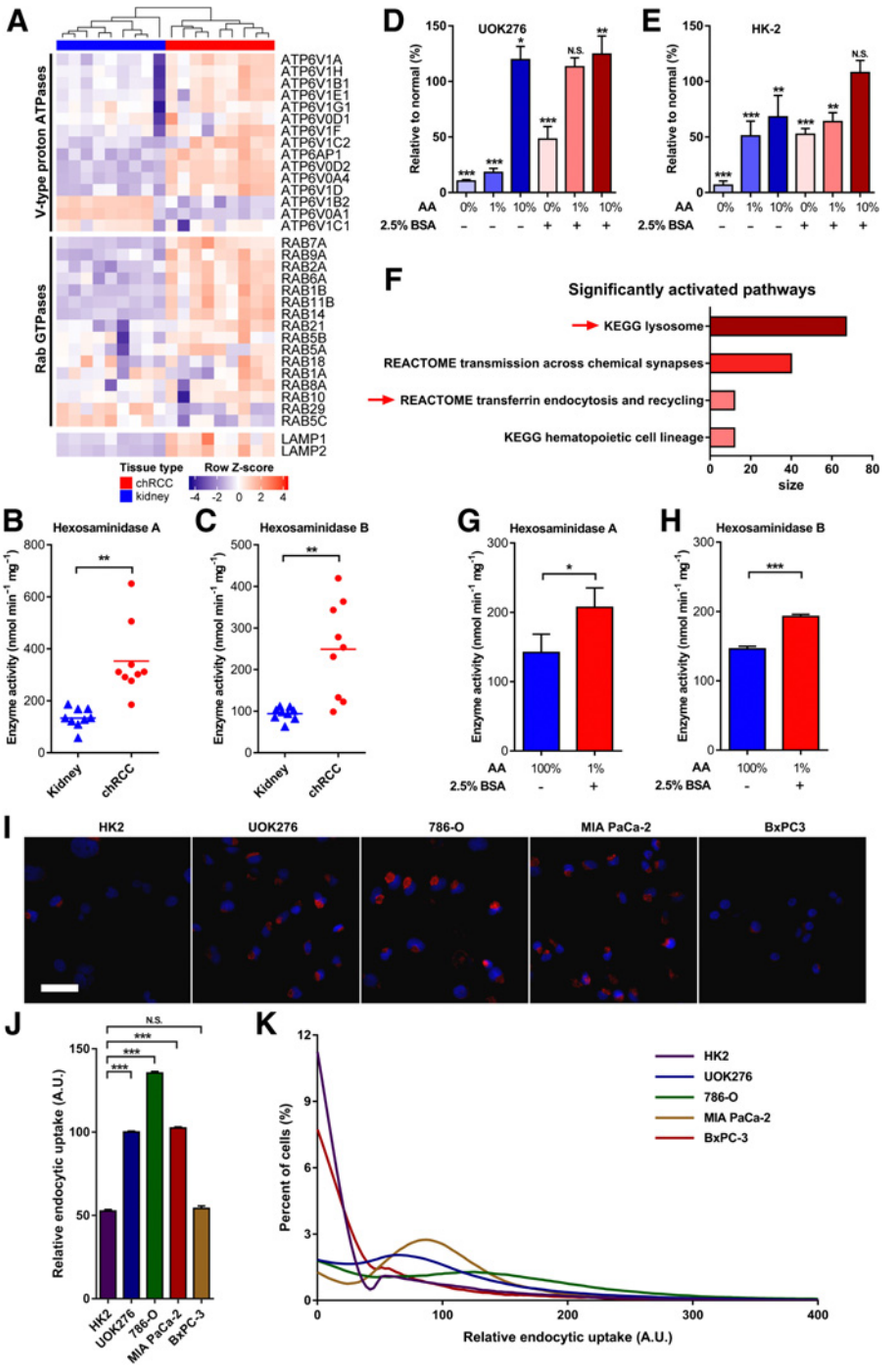

Figure 4.

chRCC cells activated endocytosis when AAs were depleted. **A,** Heatmap of quantified V-type proton ATPases, Rab GTPases, and lysosome-associated membrane protein 1 and 2 (LAMP1 and LAMP2) in chRCC and kidney tissues. The color gradient represents a relatively low (blue) or high (red) protein abundance in chRCC or normal kidney tissue. **B** and **C,** Enzymatic activities (nmol/minute/mg protein; $n = 9$) of hexosaminidase A (**B**) and B (**C**) in chRCC compared with kidney controls. **D** and **E,** Relative cell numbers of UOK276 cells (**D**) and HK2 cells (**E**) under different AA and BSA concentrations, normalized to complete medium. **F,** A pathway analysis (GSEA) of the proteome shows the upregulation of the lysosome and endocytosis in UOK276 cells in 1% AA and 2.5% BSA versus complete medium. Enriched pathway cut-off: $P < 0.01$; FDR < 0.25. **G** and **H,** Enzymatic activities (nmol/minute/mg protein; $n = 3$) of hexosaminidase A (**G**) and B (**H**) in UOK276 cells in complete medium without supplementation with BSA and 1% AAs with 2.5% BSA. The data in **D** and **E** and **G** and **H** are expressed as means ± SD. **I,** An endocytic uptake assay using DQ-Red BSA as a marker of endocytosis (red) indicates that UOK276 cells (chRCC), MIA PaCa-2 cells (*KRAS*-mutant PDAC), and 786-O cells (ccRCC) display increased levels of endocytosis compared with BxPC-3 cells (*KRAS* WT PDAC) and HK2 cells (normal human kidney). Hoechst 33432 staining (blue) identifies nuclei. (Scale bar, 50 μm.) **J,** Quantification of endocytic uptake of DQ-Red BSA in BxPC-3, MIA PaCa-2, 786-O, UOK276, and HK2 cells. Error bars indicate mean ± SEM for three independent experiments with at least 2,500 cells scored in each group. **K,** Data distribution of the relative endocytic uptake quantified in **J**. Data in **J** and **K** are presented as relative values, as the mean value of UOK276 cells was set to 100 for easy comparison. **B** and **C,** **, $P < 0.01$ by a paired *t* test; **G** and **H,** *, $P < 0.01$; **, $P < 0.01$ by a two-tailed Student *t* test. **D, E,** and **J,** *, $P < 0.01$; **, $P < 0.01$; ***, $P < 0.001$ by one-way ANOVA, with follow-up tests of each group compared with the corresponding control groups. A.U., arbitrary units. N.S., not significant.

showed that the DQ-Red BSA accumulated in UOK276 cells over time, providing evidence that macropinocytosis is an established process in chRCC cells to uptake macromolecules as nutrient source (Supplementary Movie S1). Furthermore, the endocytic uptake of DQ-Red BSA in chRCC cells (UOK276) was compared with ccRCC cells (786-O) and with normal human kidney (HK2) cells. The *KRAS* WT (BxPC-3) and $KRAS^{G12C}$ mutant (MIA PaCa-2, promotes macropinocytosis; ref. 43) pancreatic cancer cells were used as negative and positive controls, respectively. chRCC, ccRCC, and *KRAS* mutant cells showed a significantly higher endocytic uptake of DQ-Red BSA compared with *KRAS* WT and HK2 control cells (**Fig. 4I–K**). Hence, the experiments performed in the chRCC-derived UOK276 cell line validated the observation that chRCC obtains nutrients via endocytotic processes.

Pharmaceutical inhibition of the PLCG2/IP3/Ca^{2+}/PKC pathway suppresses endocytosis in chRCC cells

The protein and RNA of PLCG2 were found to be dramatically upregulated in chRCC relative to normal kidney tissue (**Fig. 5A**). PLCG2 is a membrane protein belonging to the phospholipase C

Published OnlineFirst October 28, 2020; DOI: 10.1158/0008-5472.CAN-20-1998

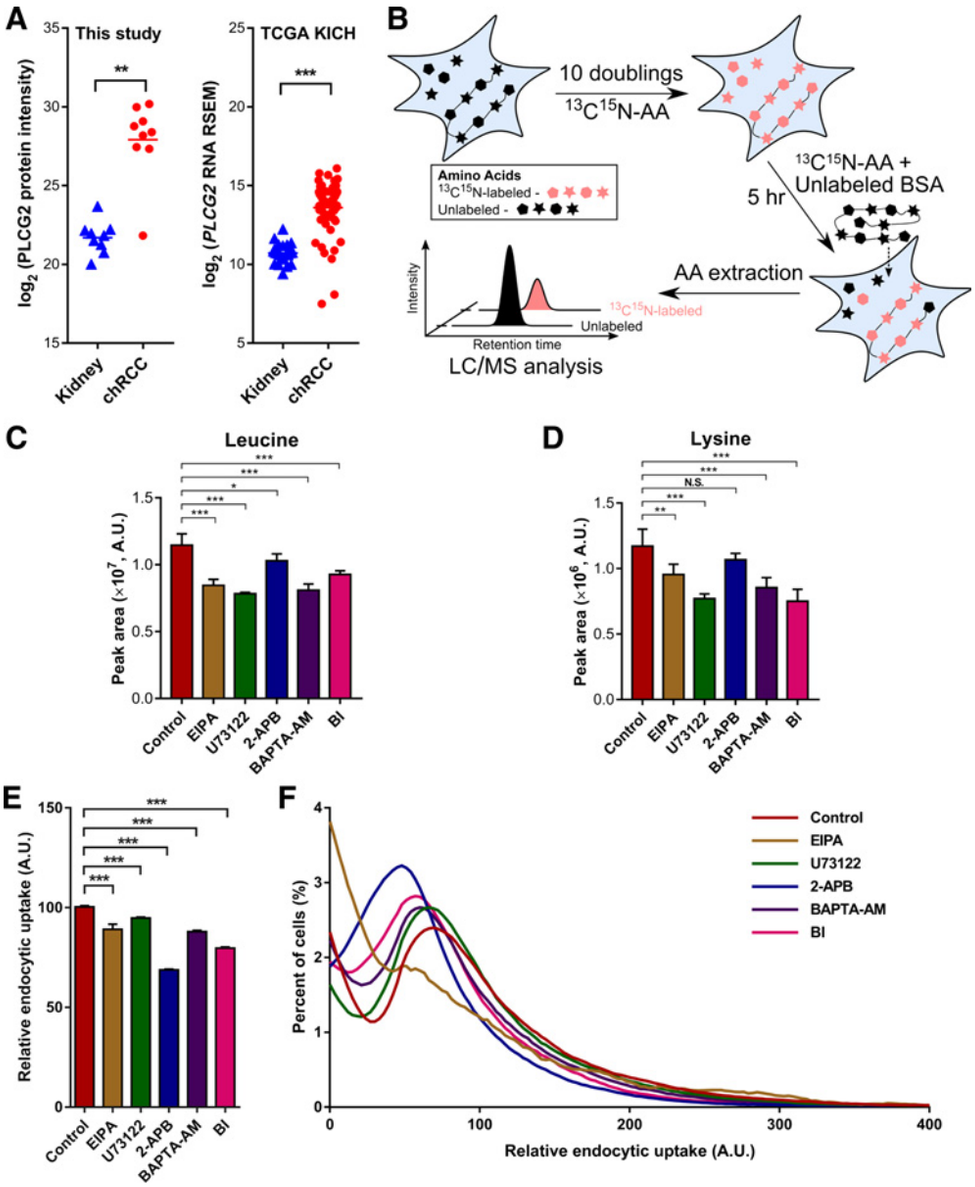

Figure 5.

Chemical inhibition of the PLCG2/IP3/Ca^{2+}/PKC pathway suppresses endocytosis in chRCC cells. **A,** log_2 protein intensity and RNA RSEM plots show that the protein and RNA abundances of PLCG2 are significantly increased in chRCC relative to normal kidney tissues. **B,** The schema displays the use of isotope tracers to quantify protein scavenging by endocytosis with mass spectrometry. **C** and **D,** The peak area plots of unlabeled (BSA-derived) leucine (**C**) and lysine (**D**) after applying 10 μmol/L EIPA, 30 μmol/L U73122, 100 μmol/L 2-APB, 30 μmol/L BAPTA-AM, and 3 μmol/L BI. **E,** Quantification of endocytic uptake of DQ-Red BSA in UOK276 cells treated with 10 μmol/L EIPA, 30 μmol/L U73122, 100 μmol/L 2-APB, 30 μmol/L BAPTA-AM, and 3 μmol/L BI. Error bars indicate mean ± SEM for three independent experiments with at least 1,000 cells scored in each group. **F,** Data distribution of the relative endocytic uptake quantified in **E**. Data in **E** and **F** are presented as relative values as the mean value of control group were set to 100 for easy comparison. *, $P < 0.05$; **, $P < 0.01$; ***, $P < 0.001$ by one-way ANOVA, with follow-up tests of each group compared with the control group. A.U., arbitrary units. N.S., not significant.

family and catalyzes the conversion of phosphatidylinositol 4,5-bisphosphate to IP3 and diacylglycerol, IP3 further activates the IP3 receptor (IP3R) on the endoplasmic reticulum to release Ca^{2+}, which further activates PCK (44). To investigate the role of PLCG2 and its downstream IP3/Ca^{2+}/PKC pathway in endocytosis, we developed an LC/MS-MS method by using isotope tracers to quantify protein scavenging by endocytosis (**Fig. 5B**). First, chRCC cells were cultured for 10 generations in medium containing ^{13}C- and ^{15}N-labeled AAs ($^{13}C^{15}N$-AA) to completely label all intracellular AAs and proteins. Then, 2.5% unlabeled BSA was added to the isotope-labeled medium, and the amount of internalized BSA in the form of derived unlabeled AAs was monitored. By measuring the amount of unlabeled essential AAs within the medium and cells, we were able to assess the endocytosis level under different conditions. EIPA (a widely used endocytosis inhibitor), U73122 (a general inhibitor of PLCG), 2-aminoethoxydiphenyl borate (2-APB, an IP3R antagonist), BAPTA-AM (a cell membrane-permeable Ca^{2+}

Published OnlineFirst October 28, 2020; DOI: 10.1158/0008-5472.CAN-20-1998

chelator), and bisindolylmaleimide I (BI, a PKC inhibitor) were applied to UOK276 cells. Leucine and lysine, the two most abundant essential AAs in BSA, were both significantly decreased in the cells treated with the mentioned inhibitors (**Fig. 5C** and **D**), and all the other essential AAs showed the same trend (Supplementary Fig. S4). To further validate the role of the PLCG2 pathway in endocytic activation, the inhibitory effect of PLCG2 pathway inhibitors on DQ-Red BSA uptake in UOK276 cells was investigated. Similar to decreased levels of essential AAs, the endocytic uptake of DQ-Red BSA in UOK276 cells was significantly lower upon inhibition (**Fig. 5E** and **F**). Taken together, these results suggest that the PLCG/IP3/Ca^{2+}/PKC pathway is involved in the activation of endocytosis in chRCC cells.

WES reveals no association of *TP53* mutations and PLCG2 expression in chRCC

Approximately 30% of all chRCC cases possess somatic mutations in the tumor suppressor gene *TP53* (5, 6). Both mutant and wild-type (WT) TP53 proteins have been reported to regulate endocytosis (45–47). We suspected that *TP53* mutations might affect the activation of endocytosis by upregulating PLCG2 expression. To test this hypothesis, WES of all chRCC tumors and their adjacent kidney tissues was performed to identify the somatic genomic mutations of chRCC in our cohort.

In total, 254 nuclear nonsynonymous variations were identified, of which, 147 were missense mutations, 13 nonsense mutations, 40 frameshift deletions, 12 frameshift insertions, 20 in-frame deletions, and 2 in-frame insertions (Supplementary Fig. S5A; Supplementary Table S2). The number of tumor-specific nuclear mutations in chRCC ranged from 16 to 53 (median of 24) per tumor (Supplementary Fig. S5B; Supplementary Table S2), which is similar to the chRCC cohort from TCGA (Supplementary Fig. S5C). In comparison with other tumor types of TCGA panel, chRCC showed a relatively low tumor mutational burden (Supplementary Fig. S5C), consistent with previous reports (5, 6). Among all identified mutations, *TP53* was found to be the most frequently mutated gene and was altered in four of nine chRCC cases, among which, two tumors exhibited nonsense mutations and two exhibited missense mutations (**Fig. 6A**; Supplementary Table S2). Surprisingly, in contrast to previous reports (5, 6), no *PTEN* mutations were identified in our cohort.

We then compared the PLCG2 protein abundance between *TP53* mutant and WT tumors. *TP53* WT tumors presented higher but statistically nonsignificant ($P = 0.056$) PLCG2 protein levels than the mutants (**Fig. 6B**). The chRCC RNA-seq dataset from TCGA, comprising a larger number of cases ($n = 66$), also showed no significant difference in PLCG2 RNA abundance between *TP53* mutants and WT tumors (**Fig. 6C**). These results suggest that the mutation status of *TP53* does not influence on the expression of PLCG2, and endocytosis in chRCC can thus be activated regardless of genetic alterations in *TP53*.

Discussion

This study employs and integrates proteomic, transcriptomic (from TCGA), and metabolomic approaches as well as WES to gain insights into the metabolic and genetic alterations in chRCC.

One hallmark of chRCC is the substantial reprogramming of central metabolic pathways. Glycolysis and gluconeogenesis share most of their enzymes, which can function in both directions, but only the abundance of gluconeogenesis-specific enzymes was significantly reduced in chRCC (up to a 1,000-fold; **Fig. 2**). Kidney is the only organ, besides liver, that can deliver anabolic glucose for the organism, but a net flux can be generated only in one direction to avoid a futile cycle, which would violate thermodynamics. All kidney tumors seem to abandon this energy-consuming pathway because similar observations were also reported at the proteome level in renal oncocytomas (16), chRCC (10), and pRCC (31) and at the transcript level in pRCC (48) and ccRCC (29). A loss of differentiation, common in cancer, is indicated by the observed changes in the abundance of these gluconeogenic proteins.

In contrast to the decrease in the abundance of gluconeogenic proteins observed in chRCC, gluconeogenic genes and proteins are frequently overexpressed in other types of tumors. Specifically, increased *ALDOB* expression was found to favor cancer cell proliferation and metastasis in multiple cancers, such as colon cancer (49), rectal cancer (50), and colorectal adenocarcinoma (51). This might also be one reason for the low metastatic potential (52) and high survival rate of patients with chRCC (53, 54). The downregulation of the FBP1, a key player in gluconeogenesis, was previously reported to be linked to ccRCC progression and was shown to inhibit nuclear HIF function (29). This further stimulates the metabolic switch by upregulating glycolytic target genes upon the loss of FBP1 in ccRCC. This increase in glycolytic enzymes in chRCC was also seen in our proteome data (**Fig. 3**). However, HIF is not involved in the regulation of glucose metabolism in chRCC. The glucose uptake is of great importance to sustain tumor growth, which was shown to be significantly lower in chRCC than in ccRCC and pRCC (12). This could be a consequence of the low microvessel density observed in chRCC compared with ccRCC tumors (11). Hence, chRCC seems to be poorly supported by classical nutrient supply chains.

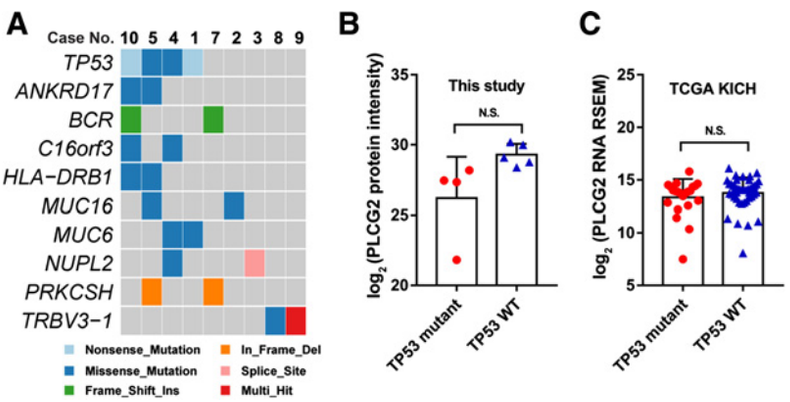

Figure 6.

TP53 mutations are not involved in the regulation of PLCG2 expression. **A,** Somatic mutations were identified by WES of chRCC and matching kidney tissues, with each column representing one sample. **B,** The $\log_2$ protein intensity of PLCG2 in *TP53* mutants and WT samples in our study ($n = 9$). **C,** The $\log_2$ RNA RSEM of PLCG2 in *TP53* mutants and WT samples from TCGA KICH study ($n = 66$). A two-tailed Student *t* test was used in **B** and **C**. N.S., not significant.

Published OnlineFirst October 28, 2020; DOI: 10.1158/0008-5472.CAN-20-1998

In addition to the dramatic reduction in enzymes involved in gluconeogenesis, decreases in the proteins of the fatty acid and AA metabolic pathways were observed in chRCC. Interestingly, the actual levels of AAs and metabolites, which can be regarded as essential "energy carriers," such as FAD, NADH, ADP, cyclic AMP, and NAD^+, were indeed unchanged (10), indicating a sufficient amount of building blocks and nutrients in chRCC. Only AA intermediates were decreased in chRCC, reflecting a lower activity of pathways involved in AA metabolism. In contrast, increased AA metabolism was frequently found in other cancer types to promote proliferation and metastasis, such as glycine and serine metabolism in breast cancer (55).

On the basis of these findings, we hypothesize that chRCC acquires nutrients preferentially in a different way. The lysosome and proteasome, which are involved in the cell recycling machinery that contributes and delivers new biomass via endocytosis, were significantly enriched. Indeed, the chRCC-derived cell line UOK276 could utilize macromolecules better under nutrient-poor conditions, and supplementation with BSA triggered a significant increase in lysosome activity. The reduced abundance of pathways involved in AA metabolism paralleled with increased abundance of the proteasome, ubiquitin-mediated proteolysis, and lysosome, suggesting that the main adaptive mechanism in chRCC involves production, recycling, and energy metabolism, such as facilitating the maintenance of proteostasis (56) or responding to stress (57).

PLCG2 was one of the most increased proteins identified by proteome profiling, and its corresponding transcript was also found to be highly upregulated in chRCC relative to healthy kidney tissues (5). Macropinosomes, which serve primarily in the uptake of solutes from the extracellular fluid (58), form as a result of macropinocytosis (known as fluid endocytosis), governed by phosphoinositides and several Rab GTPases to regulate many steps of membrane trafficking, including vesicle formation, vesicle movement, and membrane fusion (59). Consistently, most Rab GTPases were also found to be significantly increased in our chRCC specimens. During pharmaceutical inhibition of the PLCG2/IP3/Ca^{2+}/PKC pathway, a significant decrease in endocytotic processes of macromolecules was found in the chRCC cells. Furthermore, endocytosis was reported to suppress cancer cell blebbing and invasion by increasing the cell volume and membrane tension and thus decreasing the likelihood of mechanical invasion of the surrounding tissue (60). This further matches the low rate of metastatic chRCC cases (1.3%; ref. 52) and correlates with our finding of enriched endocytosis.

In summary, chRCC is characterized by substantial metabolic rewiring, with decreased gluconeogenesis and disrupted AA metabolism. We proved that activated endocytosis and subsequent increased protein degradation are necessary for chRCC to acquire nutrients from the extracellular matrix to compensate for and counteract decreased glucose uptake and AA metabolism as well as respiratory chain activities. Moreover, the PLCG2/IP3/Ca^{2+}/PKC axis plays a substantial role in the activation of endocytosis and could be targeted therapeutically in patients with chRCC.

Authors' Disclosures

J. Busch reports personal fees from MERCK, Pfizer, MSD, Roche, and Astellas outside the submitted work. M. Schütte is an employee of Alacris Theranostics GmbH. No disclosures were reported by the other authors.

Authors' Contributions

Y. Xiao: Conceptualization, data curation, formal analysis, validation, visualization, methodology, writing-original draft, writing-review and editing. **A. Rabien:** Resources, writing-review and editing. **R. Buschow:** Data curation, visualization. **V. Amstislavskiy:** Data curation. **J. Busch:** Resources. **E. Kilic:** Validation. **S.L. Villegas:** Validation. **B. Timmermann:** Resources. **M. Schütte:** Data curation. **T. Mielke:** Data curation. **M.-L. Yaspo:** Data curation. **K. Jung:** Resources, writing-review and editing. **D. Meierhofer:** Conceptualization, supervision, funding acquisition, methodology, writing-original draft, project administration, writing-review and editing.

Acknowledgments

We are thankful to Marston Linehan, from the Center for Cancer Research, Bethesda, MD, for providing the chRCC cell line UOK276 and Ulrich Keller from Charité – Universitätsmedizin Berlin for giving us the MIA PaCa-2 and BxPC-3 cell lines. Our work is supported by funds from the Max Planck Society and the China Scholarship Council to Y. Xiao and from the Foundation for Urologic Research to A. Rabien and K. Jung.

The costs of publication of this article were defrayed in part by the payment of page charges. This article must therefore be hereby marked *advertisement* in accordance with 18 U.S.C. Section 1734 solely to indicate this fact.

Received June 11, 2020; revised September 25, 2020; accepted October 20, 2020; published first October 28, 2020.

References

1. Siegel RL, Miller KD, Jemal A. Cancer statistics, 2019. CA Cancer J Clin 2019;69:7–34.
2. Bray F, Ferlay J, Soerjomataram I, Siegel RL, Torre LA, Jemal A. Global cancer statistics 2018: GLOBOCAN estimates of incidence and mortality worldwide for 36 cancers in 185 countries. CA Cancer J Clin 2018;68:394–424.
3. Moch H, Cubilla AL, Humphrey PA, Reuter VE, Ulbright TM. The 2016 WHO classification of tumours of the urinary system and male genital organs-part A: renal, penile, and testicular tumours. Eur Urol 2016;70:93–105.
4. Thoenes W, Storkel S, Rumpelt HJ, Moll R, Baum HP, Werner S. Chromophobe cell renal carcinoma and its variants–a report on 32 cases. J Pathol 1988;155:277–87.
5. Davis CF, Ricketts CJ, Wang M, Yang L, Cherniack AD, Shen H, et al. The somatic genomic landscape of chromophobe renal cell carcinoma. Cancer Cell 2014;26:319–30.
6. Durinck S, Stawiski EW, Pavia-Jimenez A, Modrusan Z, Kapur P, Jaiswal BS, et al. Spectrum of diverse genomic alterations define non-clear cell renal carcinoma subtypes. Nat Genet 2015;47:13–21.
7. Haake SM, Weyandt JD, Rathmell WK. Insights into the genetic basis of the renal cell carcinomas from The Cancer Genome Atlas. Mol Cancer Res 2016;14:589–98.
8. Brunelli M, Eble JN, Zhang S, Martignoni G, Delahunt B, Cheng L. Eosinophilic and classic chromophobe renal cell carcinomas have similar frequent losses of multiple chromosomes from among chromosomes 1, 2, 6, 10, and 17, and this pattern of genetic abnormality is not present in renal oncocytoma. Mod Pathol 2005;18:161–9.
9. Casuscelli J, Weinhold N, Gundem G, Wang L, Zabor EC, Drill E, et al. Genomic landscape and evolution of metastatic chromophobe renal cell carcinoma. JCI Insight 2017;2:e92688.
10. Xiao Y, Clima R, Busch J, Rabien A, Kilic E, Villegas SL, et al. Decreased mitochondrial DNA content drives oxphos dysregulation in chromophobe renal cell carcinoma. Cancer Res 2020;80:3830–40.
11. Jinzaki M, Tanimoto A, Mukai M, Ikeda E, Kobayashi S, Yuasa Y, et al. Double-phase helical CT of small renal parenchymal neoplasms: correlation with pathologic findings and tumor angiogenesis. J Comput Assist Tomogr 2000;24:835–42.
12. Nakajima R, Nozaki S, Kondo T, Nagashima Y, Abe K, Sakai S. Evaluation of renal cell carcinoma histological subtype and fuhrman grade using (18)F-fluorodeoxyglucose-positron emission tomography/computed tomography. Eur Radiol 2017;27:4866–73.
13. Linehan WM, Schmidt LS, Crooks DR, Wei D, Srinivasan R, Lang M, et al. The metabolic basis of kidney cancer. Cancer Discov 2019;9:1006–21.

14. Hakimi AA, Reznik E, Lee CH, Creighton CJ, Brannon AR, Luna A, et al. An integrated metabolic atlas of clear cell renal cell carcinoma. Cancer Cell 2016;29:104–16.
15. Yang Y, Vocke CD, Ricketts CJ, Wei D, Padilla-Nash HM, Lang M, et al. Genomic and metabolic characterization of a chromophobe renal cell carcinoma cell line model (UOK276). Genes Chromosomes Cancer 2017;56:719–29.
16. Kurschner G, Zhang Q, Clima R, Xiao Y, Busch JF, Kilic E, et al. Renal oncocytoma characterized by the defective complex I of the respiratory chain boosts the synthesis of the ROS scavenger glutathione. Oncotarget 2017;8:105882–904.
17. Gielisch I, Meierhofer D. Metabolome and proteome profiling of complex I deficiency induced by rotenone. J Proteome Res 2015;14:224–35.
18. Shibata H, Yagi T. Rate assay of N-acetyl-beta-D-hexosaminidase with 4-nitrophenyl N-acetyl-beta-D-glucosaminide as an artificial substrate. Clin Chim Acta 1996;251:53–64.
19. Grabowski GA, Kruse JR, Goldberg JD, Chockkalingam K, Gordon RE, Blakemore KJ, et al. First-trimester prenatal diagnosis of Tay-Sachs disease. Am J Hum Genet 1984;36:1369–78.
20. Commisso C, Flinn RJ, Bar-Sagi D. Determining the macropinocytic index of cells through a quantitative image-based assay. Nat Protoc 2014;9:182–92.
21. Koboldt DC, Zhang Q, Larson DE, Shen D, McLellan MD, Lin L, et al. VarScan 2: somatic mutation and copy number alteration discovery in cancer by exome sequencing. Genome Res 2012;22:568–76.
22. Wang K, Li M, Hakonarson H. ANNOVAR: functional annotation of genetic variants from high-throughput sequencing data. Nucleic Acids Res 2010;38:e164.
23. Albers CA, Lunter G, MacArthur DG, McVean G, Ouwehand WH, Durbin R. Dindel: accurate indel calls from short-read data. Genome Res 2011;21:961–73.
24. Goldman M, Craft B, Hastie M, Repečka K, Kamath A, McDade F, et al. The UCSC Xena Platform for cancer genomics data visualization and interpretation. bioRxiv 2019:326470. DOI: https://doi.org/10.1101/326470.
25. Li B, Dewey CN. RSEM: accurate transcript quantification from RNA-Seq data with or without a reference genome. BMC Bioinformatics 2011;12:323.
26. Tyanova S, Temu T, Sinitcyn P, Carlson A, Hein MY, Geiger T, et al. The Perseus computational platform for comprehensive analysis of (prote)omics data. Nat Methods 2016;13:731–40.
27. Subramanian A, Tamayo P, Mootha VK, Mukherjee S, Ebert BL, Gillette MA, et al. Gene set enrichment analysis: a knowledge-based approach for interpreting genome-wide expression profiles. Proc Natl Acad Sci U S A 2005;102:15545–50.
28. Vizcaino JA, Cote RG, Csordas A, Dianes JA, Fabregat A, Foster JM, et al. The PRoteomics IDEntifications (PRIDE) database and associated tools: status in 2013. Nucleic Acids Res 2013;41:D1063–9.
29. Li B, Qiu B, Lee DS, Walton ZE, Ochocki JD, Mathew LK, et al. Fructose-1,6-bisphosphatase opposes renal carcinoma progression. Nature 2014;513:251–5.
30. Priolo C, Khabibullin D, Reznik E, Filippakis H, Ogorek B, Kavanagh TR, et al. Impairment of gamma-glutamyl transferase 1 activity in the metabolic pathogenesis of chromophobe renal cell carcinoma. Proc Natl Acad Sci U S A 2018;115:E6274–E82.
31. Al Ahmad A, Paffrath V, Clima R, Busch JF, Rabien A, Kilic E, et al. Papillary renal cell carcinomas rewire glutathione metabolism and are deficient in both anabolic glucose synthesis and oxidative phosphorylation. Cancers 2019;11:1298.
32. Gopal RK, Calvo SE, Shih AR, Chaves FL, McGuone D, Mick E, et al. Early loss of mitochondrial complex I and rewiring of glutathione metabolism in renal oncocytoma. Proc Natl Acad Sci U S A 2018;115:E6283–90.
33. Xiao Y, Meierhofer D. Glutathione metabolism in renal cell carcinoma progression and implications for therapies. Int J Mol Sci 2019;20:3672.
34. Penhoet E, Rajkumar T, Rutter WJ. Multiple forms of fructose diphosphate aldolase in mammalian tissues. Proc Natl Acad Sci U S A 1966;56:1275–82.
35. Semenza GL. HIF-1 mediates the Warburg effect in clear cell renal carcinoma. J Bioenerg Biomembr 2007;39:231–4.
36. Tajima T, Goda N, Fujiki N, Hishiki T, Nishiyama Y, Senoo-Matsuda N, et al. HIF-1alpha is necessary to support gluconeogenesis during liver regeneration. Biochem Biophys Res Commun 2009;387:789–94.
37. Riazalhosseini Y, Lathrop M. Precision medicine from the renal cancer genome. Nat Rev Nephrol 2016;12:655–66.
38. Wettersten HI, Aboud OA, Lara PN Jr, Weiss RH. Metabolic reprogramming in clear cell renal cell carcinoma. Nat Rev Nephrol 2017;13:410–9.
39. Posadas EM, Limvorasak S, Figlin RA. Targeted therapies for renal cell carcinoma. Nat Rev Nephrol 2017;13:496–511.
40. Gossage L, Eisen T, Maher ER. VHL, the story of a tumour suppressor gene. Nat Rev Cancer 2015;15:55–64.
41. Tzeng HT, Wang YC. Rab-mediated vesicle trafficking in cancer. J Biomed Sci 2016;23:70.
42. Maxson ME, Grinstein S. The vacuolar-type H(+)-ATPase at a glance - more than a proton pump. J Cell Sci 2014;127:4987–93.
43. Commisso C, Davidson SM, Soydaner-Azeloglu RG, Parker SJ, Kamphorst JJ, Hackett S, et al. Macropinocytosis of protein is an amino acid supply route in Ras-transformed cells. Nature 2013;497:633–7.
44. Rhee SG, Suh PG, Ryu SH, Lee SY. Studies of inositol phospholipid-specific phospholipase C. Science 1989;244:546–50.
45. Muller PA, Caswell PT, Doyle B, Iwanicki MP, Tan EH, Karim S, et al. Mutant p53 drives invasion by promoting integrin recycling. Cell 2009;139:1327–41.
46. Yu X, Riley T, Levine AJ. The regulation of the endosomal compartment by p53 the tumor suppressor gene. FEBS J 2009;276:2201–12.
47. Sigismund S, Confalonieri S, Ciliberto A, Polo S, Scita G, Di Fiore PP. Endocytosis and signaling: cell logistics shape the eukaryotic cell plan. Physiol Rev 2012;92:273–366.
48. Cancer Genome Atlas Research Network, Linehan WM, Spellman PT, Ricketts CJ, Creighton CJ, Fei SS, et al. Comprehensive molecular characterization of papillary renal-cell carcinoma. N Engl J Med 2016;374:135–45.
49. Bu P, Chen KY, Xiang K, Johnson C, Crown SB, Rakhilin N, et al. Aldolase B-mediated fructose metabolism drives metabolic reprogramming of colon cancer liver metastasis. Cell Metab 2018;27:1249–62.e4.
50. Tian YF, Hsieh PL, Lin CY, Sun DP, Sheu MJ, Yang CC, et al. High expression of aldolase B confers a poor prognosis for rectal cancer patients receiving neoadjuvant chemoradiotherapy. J Cancer 2017;8:1197–204.
51. Li Q, Li Y, Xu J, Wang S, Xu Y, Li X, et al. Aldolase B overexpression is associated with poor prognosis and promotes tumor progression by epithelial-mesenchymal transition in colorectal adenocarcinoma. Cell Physiol Biochem 2017;42:397–406.
52. Volpe A, Novara G, Antonelli A, Bertini R, Billia M, Carmignani G, et al. Chromophobe renal cell carcinoma (RCC): oncological outcomes and prognostic factors in a large multicentre series. BJU Int 2012;110:76–83.
53. Przybycin CG, Cronin AM, Darvishian F, Gopalan A, Al-Ahmadie HA, Fine SW, et al. Chromophobe renal cell carcinoma: a clinicopathologic study of 203 tumors in 200 patients with primary resection at a single institution. Am J Surg Pathol 2011;35:962–70.
54. Amin MB, Amin MB, Tamboli P, Javidan J, Stricker H, de-Peralta Venturina M, et al. Prognostic impact of histologic subtyping of adult renal epithelial neoplasms: an experience of 405 cases. Am J Surg Pathol 2002;26:281–91.
55. Jain M, Nilsson R, Sharma S, Madhusudhan N, Kitami T, Souza AL, et al. Metabolite profiling identifies a key role for glycine in rapid cancer cell proliferation. Science 2012;336:1040–4.
56. Zhang Y, Manning BD. mTORC1 signaling activates NRF1 to increase cellular proteasome levels. Cell Cycle 2015;14:2011–7.
57. Livneh I, Cohen-Kaplan V, Cohen-Rosenzweig C, Avni N, Ciechanover A. The life cycle of the 26S proteasome: from birth, through regulation and function, and onto its death. Cell Res 2016;26:869–85.
58. Racoosin EL, Swanson JA. Macropinosome maturation and fusion with tubular lysosomes in macrophages. J Cell Biol 1993;121:1011–20.
59. Stenmark H. Rab GTPases as coordinators of vesicle traffic. Nat Rev Mol Cell Biol 2009;10:513–25.
60. Holst MR, Vidal-Quadras M, Larsson E, Song J, Hubert M, Blomberg J, et al. Clathrin-independent endocytosis suppresses cancer cell blebbing and invasion. Cell Rep 2017;20:1893–905.

Published OnlineFirst October 28, 2020; DOI: 10.1158/0008-5472.CAN-20-1998

Cancer Research
The Journal of Cancer Research (1916–1930) | The American Journal of Cancer (1931–1940)

AACR American Association for Cancer Research

Endocytosis-Mediated Replenishment of Amino Acids Favors Cancer Cell Proliferation and Survival in Chromophobe Renal Cell Carcinoma

Yi Xiao, Anja Rabien, René Buschow, et al.

Cancer Res 2020;80:5491-5501. Published OnlineFirst October 28, 2020.